Check for updates

Single-Molecule Conductance

International Edition: DOI: 10.1002/anie.201915200
German Edition: DOI: 10.1002/ange.201915200

Controlling Single Molecule Conductance by a Locally Induced Chemical Reaction on Individual Thiophene Units

Tomasz Michnowicz[+], Bogdana Borca[+], Rémi Pétuya[+], Verena Schendel, Marcel Pristl, Ivan Pentegov, Ulrike Kraft, Hagen Klauk, Peter Wahl, Pingo Mutombo, Pavel Jelínek, Andrés Arnau, Uta Schlickum,* and Klaus Kern*

Abstract: *Among the prerequisites for the progress of single-molecule-based electronic devices are a better understanding of the electronic properties at the individual molecular level and the development of methods to tune the charge transport through molecular junctions. Scanning tunneling microscopy (STM) is an ideal tool not only for the characterization, but also for the manipulation of single atoms and molecules on surfaces. The conductance through a single molecule can be measured by contacting the molecule with atomic precision and forming a molecular bridge between the metallic STM tip electrode and the metallic surface electrode. The parameters affecting the conductance are mainly related to their electronic structure and to the coupling to the metallic electrodes. Here, the experimental and theoretical analyses are focused on single tetracenothiophene molecules and demonstrate that an in situ-induced direct desulfurization reaction of the thiophene moiety strongly improves the molecular anchoring by forming covalent bonds between molecular carbon and copper surface atoms. This bond formation leads to an increase of the conductance by about 50 % compared to the initial state.*

One of the challenges associated with reducing electronic circuits to single-molecule components is the formation of reliable, low-resistance contacts between the molecule and the metallic electrodes to enable an efficient charge transport across the metal–organic interface.[1,2] While π-conjugated systems with a delocalized electronic structure are typically characterized by a high electronic conductance through the molecules,[3,4] they are usually equipped with non-conjugated end groups designed to selectively couple the molecules to specific metallic electrodes.[5–7] Moreover, the ability to control the junction's geometry with the spatial overlap of orbitals is an important prerequisite for the optimization of the electronic device properties, such as the charge-injection efficiency and the charge mobility.[8–11] To this end, covalent bonds between the molecule and the metal electrodes are advantageous to ensure a robust mechanical and electronic connection. In the ideal case, the organo–metallic contacts of the molecular electronic element are established through a chemical reaction between the molecule and the metal. The

[*] Dr. T. Michnowicz,[+] Dr. B. Borca,[+] Dr. V. Schendel, M. Pristl, Dr. I. Pentegov, Prof. P. Wahl, Prof. U. Schlickum, Prof. K. Kern
Department of Nanoscale Science
Max Planck Institute for Solid State Research
Heisenbergstrasse 1, 70569 Stuttgart (Germany)

Dr. U. Kraft, Dr. H. Klauk
Department of Organic Electronics
Max Planck Institute for Solid State Research
Heisenbergstrasse 1, 70569, Stuttgart (Germany)

Dr. B. Borca[+]
National Institute of Materials Physics
Atomistilor Strasse, No. 405A, 077125, Magurele (Romania)
E-mail: bogdana.borca@infim.ro

Dr. R. Pétuya,[+] Prof. A. Arnau
Institution: Donostia International Physics Centre
Paseo Manuel de Lardizabal 4
20018 Donostia—San Sebastián (Spain)

Prof. P. Wahl
SUPA, School of Physics and Astronomy, University of St Andrews
North Haugh, St Andrews, KY16 9SS (UK)

Dr. P. Mutombo, Dr.-Ing. P. Jelínek
Nanosurf Lab, Institute of Physics of the Czech Academy of Science
Cukrovarnicka 10, 16253 Praha 6 (Czech Republic)

Prof. A. Arnau
UPV/EHU and Material Physics Center (MPC)
Centro Mixto CSIC-UPV/EHU
Paseo Manuel de Lardizabal 5
20018 Donostia—San Sebastián (Spain)

Prof. U. Schlickum
Institute of Applied Physics, Technische Universität Braunschweig
Mendelssohnstraße 2, 38106 Braunschweig (Germany)
E-mail: u.schlickum@tu-bs.de

Prof. K. Kern
Institut de Physique
École Polytechnique Fédérale de Lausanne (EPFL)
EPFL SB IPHYS-Direction Bâtiment PH, Station 3
1015 Lausanne (Switzerland)

Dr. R. Pétuya[+]
Present address: University of Liverpool, Department of Chemistry
Crown Street, Liverpool L69 7ZD (UK)

Dr. U. Kraft
Present address: University of Cambridge, Cavendish Laboratory
J J Thomson Avenue, Cambridge, CB3 0HE (UK)

Dr. B. Borca[+]
Present address: Institute of Applied Physics
Technische Universität Braunschweig
Mendelssohnstrasse 2, 38106 Braunschweig (Germany)

[+] These authors contributed equally to this work.

Supporting information and the ORCID identification number(s) for the author(s) of this article can be found under: https://doi.org/10.1002/anie.201915200.

© 2020 The Authors. Published by Wiley-VCH Verlag GmbH & Co. KGaA. This is an open access article under the terms of the Creative Commons Attribution Non-Commercial NoDerivs License, which permits use and distribution in any medium, provided the original work is properly cited, the use is non-commercial, and no modifications or adaptations are made.

most popular examples are systems with covalent bonds formed between sulfur-containing molecular end groups and gold electrodes.[4] When the anchoring is realized through direct covalent bonds between the carbon atoms and the metal, a higher electronic conductance is obtained[4,12] due to a stronger coupling between the metal and the molecular π-system and a greater overlap of metal and molecular wave functions. The most common methods used to measure the electronic properties of organic molecules are based on the formation of break junctions[13] by trapping the molecules between contacts. This technique can be realized in mechanically controlled break junctions, and in a more controlled way in scanning tunneling microscopes (STM)[14] or in conductive atomic force microscopes (AFM).[15] Variations of the molecular geometry and the number of molecules in the junction as well as the significant effects of the local environment may lead to very different signatures in the conductance even for the same molecular species. To avoid these uncertainties, we use an STM operating under ultra-high vacuum conditions and at low temperature. The instrument is particularly suitable for performing accurate conductance measurements through single molecules, as it allows us to characterize the structure at the submolecular level[16–19] and to atomically precisely contact one specific end of the molecular unit with the tip apex.[20–25]

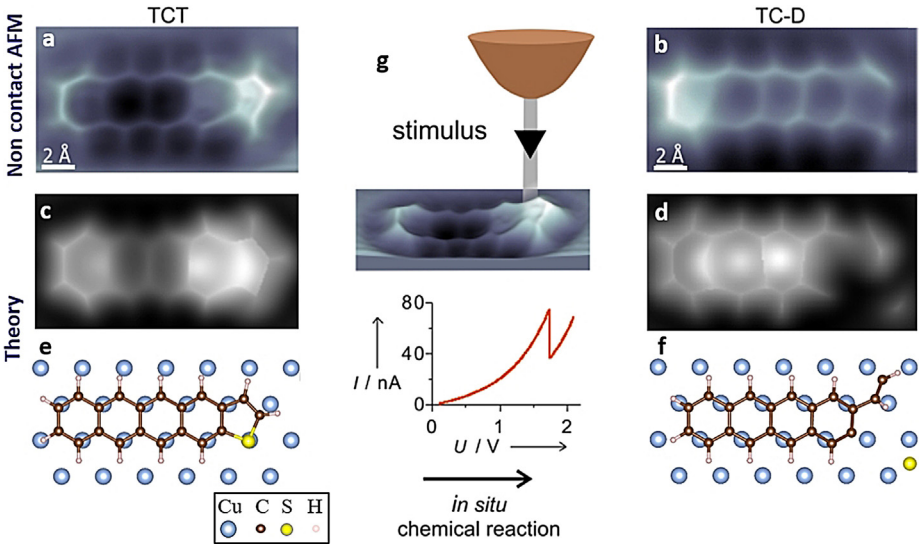

Figure 1. Controlled desulfurization reaction. a) and b) AFM frequency-shift images of tetraceno-thiophene (TCT) and tetraceno-derivative (TC-D) molecules, respectively. c) and d) Simulated AFM images based on DFT calculations. e) and f) Adsorption geometry of the surface-molecule structure obtained from DFT calculations in a ball-and-stick representation. g) Schematic representation of the experiment; the reaction produces a step-like feature in the I(V) trace recorded at a constant height above the thiophene unit.

Here we explore a new class of covalent bond formation between a chemically reacted thiophene molecular end group and Cu electrodes. We investigate the molecule-metal-electrode anchoring and the conductance across a tetracenothiophene (TCT) molecule, a pentacene analogue, by controlling the formation of covalent C–Cu bonds between the molecule and the metal substrate on the submolecular scale. We demonstrate in this work that the resulting tetraceno derivative (TC-D) shows a significant increase in the conductance, as a result of a better contact formation between the bifurcated end of the remaining thiophene part and the metal surface, whose fingerprint is an intramolecular enhancement of the local density of states close to the Fermi energy.

Previously we have shown[26] an in situ induced direct desulfurization reaction on single thiophene units on Cu(111) surfaces driven by the electric field confined in the tunnel junction (Figure 1). This desulfurization reaction of the TCT molecules can also be induced thermally (see Supporting Information 2 for details). We now included high-resolution non-contact AFM (nc-AFM) images clearly revealing the opening of the thiophene ring and the split-off of the S-atom. Using a CO-functionalized tip for non-contact AFM, we are sensitive to the potential energy basins produced by the Pauli repulsion between the CO-terminated tip apex and specific atomic positions within adsorbed molecules.[27] This methodology gives rise to an extremely high resolution of intermolecular structures.[28] The high-resolution nc-AFM images of TCT and TC-D as well as simulated nc-AFM images obtained from DFT calculations clearly uncover the inter-molecular structure before and after the chemical surface reaction (Figure 1).

As a consequence of this reaction, the two carbon atoms formerly connected to the S atom in the thiophene group bind covalently to Cu surface atoms, while the S atom is irreversibly detached from the molecule. The resulting molecule, a tetraceno derivative (TC-D) is therefore anchored to the surface by two covalent bonds.

To probe the effect of the strong anchoring of one of the molecule's end groups to the metal electrode, we performed conductance measurements through single TCT and TC-D molecules. The geometry of the measurement is sketched schematically in Figure 2. Before each conductance measurement, the molecule is first imaged by STM. Then, the tip is placed on top of the acene termination of the molecule, the feedback loop is switched off and the tip is moved towards the molecule while the current is recorded as a function of the tip-sample displacement (z). At the jump-to-contact position we obtain the conductance in units of the conductance quantum $G_0 = 2e^2h^{-1} = 77.5\ \mu S$. Figure 2a shows an example of such a $G(z)$ curve. The exponential increase of the conductance corresponding to the tunneling regime is due to the reduction of the width of the tunneling barrier.

At a certain distance of the tip above the molecule, an abrupt increase in conductance is observed with a step-like

 © 2020 The Authors. Published by Wiley-VCH Verlag GmbH & Co. KGaA, Weinheim

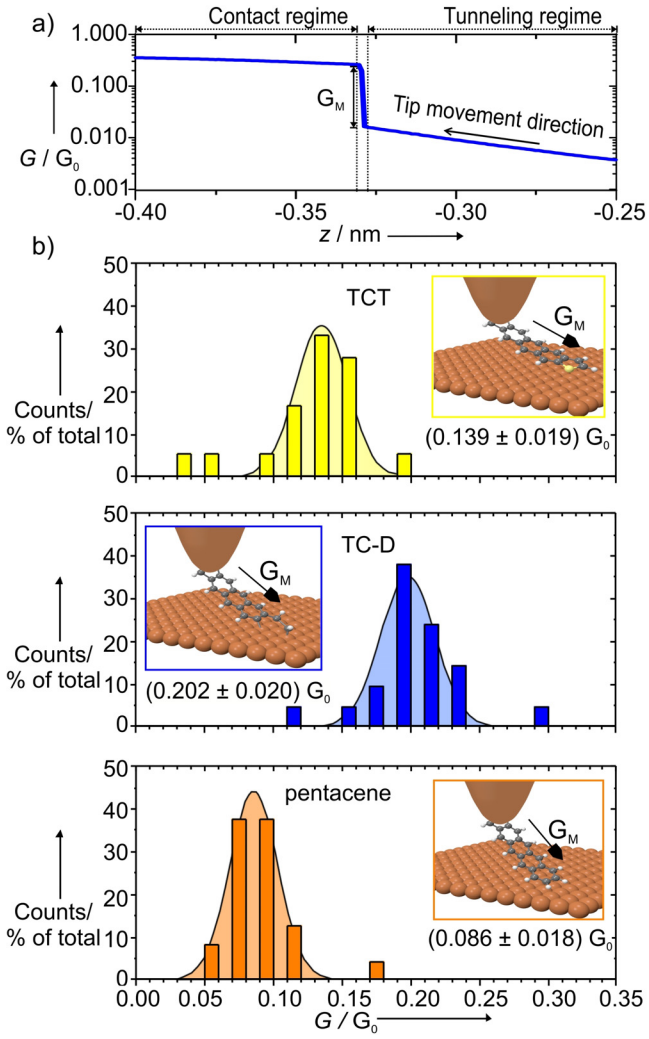

Figure 2. Conductance measurements through single molecules. a) G(z) curves acquired after switching the feedback loop off at a set point: $I = 100$ pA, $V = 100$ mV and approaching the tip 400 pm towards the molecule (only last 150 pm of the approach depicted). Initially, the measured conductance corresponds to the tunneling current (tunneling regime). Upon the approach, a tip-molecule contact is realized and the recorded conductance corresponds to the sum of direct current passing through the molecule and a tunneling current between tip and Cu-surface (contact regime). The conductance through the molecular system G_M is obtained by subtracting the tunneling conductance measured just before the jump-to-contact from the value measured just after the jump-to-contact. The curve shown was acquired on a TC-D molecule contacted on the acene side. b) Conductance histograms (with a binning of ± 0.01 G_0; all data points are obtained at the same bias voltage ($V = 100$ mV) and at small snap-to-contact window (z distance between 315 and 365 pm. We show the data of pentacene analogues TCT and TC-D and added for comparison pure pentacene. The error bar corresponds to the standard deviation extracted from the Gaussian fit. Insets: Schematic representation of the measurement configuration.

feature (Figure 2a). This corresponds to the jump-to-contact of the molecular moiety to the tip apex and indicates lifting-up of this part of the molecule from the surface. We speculate that the contact of the terminal acene ring to the tip is formed through the molecular π-orbitals. The conductance through the molecular system (G_M) is extracted from the step height in the jump-to-contact regime (Figure 2a). Each conductance measurement was performed on a different molecule. The jump-to-contact behavior can occur at different tip-sample distances. To reduce the influence of the geometry of the junction with the molecule lifted from the surface on the conductance comparison, we only considered data obtained within a small tip-distance window of 50 pm (see Supporting Information 4 for details). All these conductance values G_M for TCT and TC-D are summarized in the histograms in Figure 2b. Since TCT is a pentacene analogue, we also added as a reference the values measured for pure pentacene. The average conductance values for TC-D are significantly larger; they are more than 45% higher compared with TCT and 130% compared to pentacene. The broad conductance distributions reflect the variation in the bonding geometries at the contact with the tip and different tip geometries encountered in different experiments.

We attribute the differences between the conductance through the different types of molecules (TCT, TC-D, pentacene) to variations of the molecule-metal interaction strength together with changes in the molecular electronic structure. These effects are further analyzed using DFT calculations, in particular by comparing the electronic structure and the degree of the hybridization of the molecules to the Cu surface atoms (Figure 3). The conduction of the molecular junction is mainly determined by the electronic structure close to the Fermi level and by the transmission eigenchannels through the calculated molecular structures (ensuring a low molecular resistance).

In Figure 3a we show the partial charge densities of each type of molecule, as defined in the figure caption by energy integration around the Fermi level. For all three molecules the spatial distribution of the electronic charge shown in Figure 3a is rather uniform along the tetracene part. However, there is a significant difference on the reacted thiophene side of the TC-D molecule. The locally driven desulfurization reaction leads to the formation of covalent bonds between the bifurcated termination and the copper surface. The covalent bond formation results in a strong increase in the overlap of the wave functions between the metal electrode and the molecular end group, thus inducing a strong anchoring process that may also induce a reduction of the contact resistance (for details see Supporting Information 5). The strong coupling between the molecular end group and the surface atoms is also evidenced in the experiments by the fact that the reacted molecule cannot be picked up completely with the STM tip apex by STM manipulation, whereas this is possible for TCT and pentacene molecules.

In order to correlate the changes of the conductance to the intrinsic molecular properties, we calculated the projected density of states (PDOS) by summing over the atoms on different parts of the molecules (Figures 3b and c). An overall enhancement of the PDOS close to the Fermi level (E_F) of the metal is observed on the entire TC-D molecule, which is related to the electronic-density delocalization of the aromatic system, but it is most significant at the thiophene side (side 2) compared to pentacene and TCT. The enhancement of the PDOS close to E_F for TC-D is responsible for the

 © 2020 The Authors. Published by Wiley-VCH Verlag GmbH & Co. KGaA, Weinheim

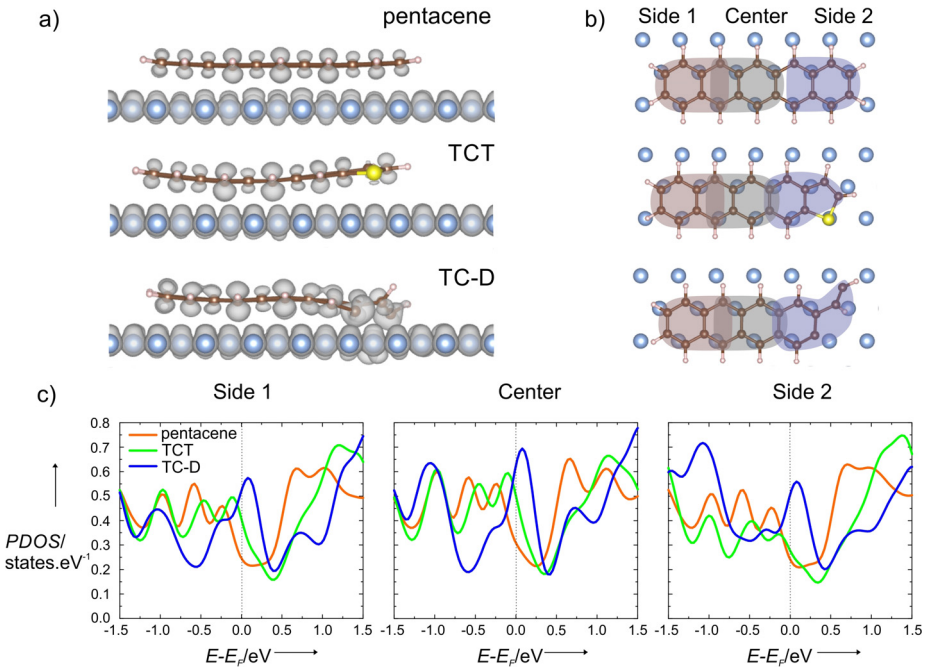

Figure 3. Calculated electronic structure and adsorption conformation of pentacene, TCT and TC-D molecules on Cu(111). a) Side views of the electronic partial charge densities after an energy integration in the interval [−0.5;0.5] eV around the Fermi level. The corresponding isocontour value is 0.004 e Bohr^{-3} for the converged molecular structures represented on ball-and-stick models of the pentacene, TCT and TC-D molecules. b) Ball-and-stick representation of the molecules considering different moieties for the calculation of the projected density of states (PDOS). c) PDOS on different sides of the molecules summing over 8 carbon atoms for pentacene, TCT and TC-D, respectively.

higher transmission, especially at the contact formation at side 2.

In conclusion, we have demonstrated a significant increase in the conductance (about 50%) through a single molecular junction by a controlled direct desulfurization reaction on one single thiophene unit. As a consequence of the chemical reaction, covalent bonds are formed between the bifurcated end of the reacted thiophene part and Cu surface atoms. This strongly enhances the electronic and mechanical anchoring to the substrate and reduces the contact resistance between the molecular end group and the metal substrate. The augmented overlap of the wave functions results in an overall increase of the density of states close to the Fermi level, in particular at the thiophene side, and in an increase of the conductivity through single TC-D molecules. These results pave the way toward a new approach for an efficient molecule-metal-electrode anchoring resulting in a drastic increase in conductance essential for single-molecule electronic device elements.

Experimental Section

Experimental Details: Experiments were performed under ultra-high-vacuum (UHV) conditions. The substrate is a Cu(111) surface, which was cleaned by repeated cycles of Ar+ ion bombardment and subsequent annealing at 800 K. Pentacene was purchased from Sigma–Aldrich. TCT molecules were synthesized following the methodology described in reference [29]. The spectroscopic investigations of the identity and purity of tetracenothiophene and the precursors is presented in the Supporting Information 1. The pentacene and TCT molecules were thermally sublimated separately and in different experiments from ceramic crucibles at 445 K and 485 K, respectively. The molecular coverage in different experiments was between 7 to 15% of a monolayer. We have always selected isolated molecules for the conductance measurements which is one of the advantages using STM. For the pentacene sublimation, the substrate was at room temperature, while for TCT the Cu(111) surface was held at 200–250 K during deposition to avoid the thermally induced desulfurization (see Supporting Information 2). After each evaporation, the sample was transferred in situ into the STM, operating at low temperatures (6 K). The STM measurements were carried out by applying the bias voltages to the sample. The TC-D molecules were produced in the STM by the direct desulfurization reaction, performed by placing the tip on top of the thiophene moiety of a TCT molecule, at a height corresponding to the set point of 100 pA, 100 mV. Then, the feedback loop was switched off and at constant height the voltage was ramped. Changes in the $I(V)$ curves were observed when the reaction occurred. The high-resolution nc-AFM frequency-shift images were acquired with a CO-terminated tip. The CO molecule was vertically manipulated to the tip apex from the NaCl(100) islands. For the AFM image acquisition, the tip was positioned over the thiophene group in the case of the TCT molecule and over the tetracene termination in the case of the TC-D molecule. At the feedback 150 pA and 10 mV, the STM Z-feedback was switched off and the bias voltage was reduced to 1 mV. The images were obtained with both amplitude and phase feedback of the AFM enabled and using the oscillation amplitude of 40 pm. The conductance measurements were performed by a vertical manipulation procedure. After switching off the feedback loop at 100 pA, 100 mV and moving the tip toward the molecules by 250 pm, the $I(z)$ curves were recorded above the acene-terminated end of each molecule, which were identified beforehand locally by imaging the molecule in the STM mode. STM images of a TCT molecule and of the produced TC-D molecules are shown in Supporting Information 3.

Computational Methods: DFT-vdW calculations were performed using the Vienna Ab-initio Simulation Package (VASP).[30,31] An (8 × 6) periodic supercell with a 4-layer slab was employed to model the adsorption of each type of molecule (TCT, TC-D, pentacene) on the Cu(111) surface. For each geometry optimization, full relaxation of all degrees of freedom of the molecule's atoms was performed, and the projected densities of states (PDOS) over the p_z orbitals of the carbon atoms were computed for the equilibrium geometries. Ion-electron interactions were described with the projector augmented-wave (PAW) method,[32] and the exchange correlation was modelled within the generalized gradient approximation (GGA).[33] Van-der-Waals dispersion forces were included using the vdW-DF-cx method.[34,35] It is worth mentioning that with this functional we obtained a 2.38 Å adsorption distance of pentacene on Cu(111), in good agreement with experimental findings of 2.34 ± 0.02 Å.[36] We

 © 2020 The Authors. Published by Wiley-VCH Verlag GmbH & Co. KGaA, Weinheim

considered a 500 eV energy cutoff in the plane-wave expansion, with a 2×3 k-point mesh in the 1×1 unit cell as sampling of the Brillouin zone reciprocal space. The electronic convergence criterion was 1×10^{-4} for all static calculations, and the convergence on forces in the relaxations was 0.05 eV Å^{-1}. The VESTA software[37] was employed for the ball-and-stick and charge density representations.

From the DFT-vdW optimized adsorptions geometries, AFM image simulations were performed using the probe-particle model,[27,38] which is based on the van-der-Waals (vdW) and electrostatic interactions between the sample and the tip. The electrostatic interaction between tip and sample was calculated from the surface Hartree potential obtained from DFT calculations, while the classic pairwise potential (Lenard–Jones) was used to describe the Van-der-Waals attraction and the Pauli repulsion. The AFM calculations were carried out with different values of the effective charge of the probe particle in order to obtain AFM images that show a good agreement with the experimental results. It was found that a quadrupole (d_{z^2}) distribution of the effective charge was more appropriate to describe the CO-terminated tip.[39] Note that all theoretical simulations were performed with a fixed lateral stiffness of $(k)=0.25\,\mathrm{N\,m^{-1}}$ and by approximating the CO-functionalized tip by an effective atomic radius $R_c=1.661$ Å. The agreement between the theoretical findings and the experiments enables us to understand and interpret the origin of the chemical contrast.

Acknowledgements

The authors acknowledge the Emmy-Noether-Program of the Deutsche Forschungsgemeinschaft, the SFB 767, Core Program PN19-03 (contract number 21 N/08.02.2019) founded by the Romanian Ministry of Research and Innovation, Basque Departamento de Universidades e Investigación (grant no. IT-756-13), the Spanish Ministerio de Economía *y* Competitividad (grant no. FIS2013-48286-C2-8752-P and FIS2016-75862-P) and the Operational Programme Research, Development and Education financed by European Structural and Investment Funds and the Czech Ministry of Education, Youth and Sports (Project No. SOLID21 CZ.02.1.01/0.0/0.0/16_019/0000760). P.M. and P.J. acknowledge access to computing and storage facilities owned by parties and projects contributing to the Czech National Grid Infrastructure MetaCentrum provided under the programme "Projects of Large Research, Development, and Innovations Infrastructures" (CESNET LM2015042). P.J. acknowledges support from Praemium Academie of the Academy of Science of the Czech Republic and MEYS LM2015087.

Conflict of interest

The authors declare no conflict of interest.

Keywords: covalent-bond formation · DFT · single-molecule conductance · STM/AFM · strong anchoring

How to cite: *Angew. Chem. Int. Ed.* **2020**, *59*, 6207–6212
Angew. Chem. **2020**, *132*, 6266–6271

[1] "Unimolecular Electronic Devices": R. M. Metzger, D. L. Mattern, *Unimolecular and Supramolecular Electronics II* (Eds.: R. M. Metzger, D. L. Mattern), Springer Berlin Heidelberg, Berlin, **2011**, pp. 39–84.
[2] N. J. Tao, *Nat. Nanotechnol.* **2006**, *1*, 173–181.
[3] "Molecular Electronic Junction Transport: Some Pathways and Some Ideas": G. C. Solomon, C. Herrmann, M. A. Ratner, *Unimolecular and Supramolecular Electronics II* (Eds.: R. M. Metzger, D. L. Mattern), Springer Berlin Heidelberg, Berlin, **2011**, pp. 1–38.
[4] T. A. Su, M. Neupane, M. L. Steigerwald, L. Venkataraman, C. Nuckolls, *Nat. Rev. Mater.* **2016**, *1*, 16002.
[5] A. Nitzan, M. A. Ratner, *Science* **2003**, *300*, 1384–1389.
[6] F. Chen, X. Li, J. Hihath, Z. Huang, N. Tao, *J. Am. Chem. Soc.* **2006**, *128*, 15874–15881.
[7] K. Moth-Poulsen, T. Bjørnholm, *Nat. Nanotechnol.* **2009**, *4*, 551–556.
[8] A. Kahn, N. Koch, W. Y. Gao, *J. Polym. Sci. Part A J. Polym. Sci. B* **2003**, *41*, 2529–2548.
[9] H. Ishii, K. Sugiyama, E. Ito, K. Seki, *Adv. Mater.* **1999**, *11*, 605–625.
[10] W. R. Silveira, J. A. Marohn, *Phys. Rev. Lett.* **2004**, *93*, 116104.
[11] N. Koch, *ChemPhysChem* **2007**, *8*, 1438–1455.
[12] G. Foti, H. Vázquez, D. Sánchez-Portal, A. Arnau, T. Frederiksen, *J. Phys. Chem. C* **2014**, *118*, 27106–27112.
[13] M. A. Reed, C. Zhou, C. J. Muller, T. P. Burgin, J. M. Tour, *Science* **1997**, *278*, 252–254.
[14] B. Xu, N. J. Tao, *Science* **2003**, *301*, 1221–1223.
[15] X. D. Cui, A. Primak, X. Zarate, J. Tomfohr, O. F. Sankey, A. L. Moore, T. A. Moore, D. Gust, G. Harris, S. M. Lindsay, *Science* **2001**, *294*, 571–574.
[16] J. Repp, G. Meyer, S. M. Stojković, A. Gourdon, C. Joachim, *Phys. Rev. Lett.* **2005**, *94*, 026803.
[17] R. Temirov, S. Soubatch, O. Neucheva, A. C. Lassise, F. S. Tautz, *New J. Phys.* **2008**, *10*, 053012.
[18] J. Brede, N. Atodiresei, S. Kuck, P. Lazić, V. Caciuc, Y. Morikawa, G. Hoffmann, S. Blügel, R. Wiesendanger, *Phys. Rev. Lett.* **2010**, *105*, 047204.
[19] L. Gross, N. Moll, F. Mohn, A. Curioni, G. Meyer, F. Hanke, M. Persson, *Phys. Rev. Lett.* **2011**, *107*, 086101.
[20] C. Joachim, J. K. Gimzewski, R. R. Schlittler, C. Chavy, *Phys. Rev. Lett.* **1995**, *74*, 2102.
[21] A. Yazdani, D. M. Eigler, N. D. Lang, *Science* **1996**, *272*, 1921.
[22] G. Schull, T. Frederiksen, M. Brandbyge, R. Berndt, *Phys. Rev. Lett.* **2009**, *103*, 206803.
[23] Y. H. Zhang, P. Wahl, K. Kern, *Nano Lett.* **2011**, *11*, 3838–3843.
[24] S. Schmaus, A. Bagrets, Y. Nahas, T. K. Yamada, A. Bork, M. Bowen, E. Beaurepaire, F. Evers, W. Wulfhekel, *Nat. Nanotechnol.* **2011**, *6*, 185–189.
[25] L. Vitali, R. Ohmann, K. Kern, A. Garcia-Lekue, T. Frederiksen, D. Sanchez-Portal, A. Arnau, *Nano Lett.* **2010**, *10*, 657–660.
[26] B. Borca, T. Michnowicz, R. Pétuya, M. Pristl, V. Schendel, I. Pentegov, U. Kraft, H. Klauk, P. Wahl, R. Gultzer, A. Arnau, U. Schlickum, K. Kern, *ACS Nano* **2017**, *11*, 4703–4709.
[27] P. Hapala, G. Kichin, C. Wagner, F. S. Tautz, R. Temirov, P. Jelínek, *Phys. Rev. B* **2014**, *90*, 085421.
[28] L. Gross, F. Mohn, N. Moll, P. Liljeroth, G. Meyer, *Science* **2009**, *325*, 1110–1114.
[29] U. Kraft, J. E. Anthony, E. Ripaud, M. A. Loth, E. Weber, H. Klauk, *Chem. Mater.* **2015**, *27*, 998–1004.
[30] G. Kresse, J. Hafner, *Phys. Rev. B* **1994**, *49*, 14251–14269.
[31] G. Kresse, J. Furthmuller, *Phys. Rev. B* **1996**, *54*, 11169–11186.
[32] P. E. Blöchl, *Phys. Rev. B* **1994**, *50*, 17953–17979.
[33] J. P. Perdew, K. Burke, M. Ernzerhof, *Phys. Rev. Lett.* **1996**, *77*, 3865; Erratum: J. P. Perdew, K. Burke, M. Ernzerhof, *Phys. Rev. Lett.* **1997**, *78*, 1396–1396.
[34] K. Berland, P. Hylgaard, *Phys. Rev. B.* **2014**, *89*, 035412.
[35] T. Björkman, *J. Chem. Phys.* **2014**, *141*, 074708.

 © 2020 The Authors. Published by Wiley-VCH Verlag GmbH & Co. KGaA, Weinheim

[36] N. Koch, A. Gerlach, S. Duhm, H. Glowatzki, G. Heimel, A. Vollmer, F. Schreiber, *J. Am. Chem. Soc.* **2008**, *130*, 7300 – 7304.
[37] K. Momma, F. Izumi, *J. Appl. Crystallogr.* **2011**, *44*, 1272 – 1276.
[38] P. Hapala, R. Temirov, F. S. Tautz, P. Jelínek, *Phys. Rev. Lett.* **2014**, *113*, 226101.
[39] J. Peng, J. Guo, P. Hapala, D. Cao, R. Ma, B. Cheng, L. Xu, M. Odráček, P. Jelínek, E. Wang, Y. Jiang, *Nat. Commun.* **2018**, *9*, 122.

Manuscript received: November 28, 2019
Revised manuscript received: January 4, 2020
Accepted manuscript online: January 22, 2020
Version of record online: February 18, 2020

 © 2020 The Authors. Published by Wiley-VCH Verlag GmbH & Co. KGaA, Weinheim

Table of Contents

1. Synthesis and purity analysis of product and precursors

The identity and purity of tetracenothiophene and the precursors was verified by elemental analysis, mass spectrometry and NMR spectroscopy (Varian Unity 400 MHz). ^{1}H chemical shifts and ^{13}C shifts were referenced to CDCl3 (7.27 ppm and 77.0 ppm).

Tetraceno[2,3-*b*]thiophene

Tetraceno[2,3-*b*]thiophene was obtained by reducing tetraceno[2,3-b]thiophene-5,12-dione using NaBH4 and subsequently SnCl2/10% HCl (see reference [SI1]).

Elemental composition: calc.: C: 84.47 %, H: 4.25 %, S: 11.28 %
found: C: 84.40 %, H: 4.31 %, S: 11.30 %

Mass spectrometry:

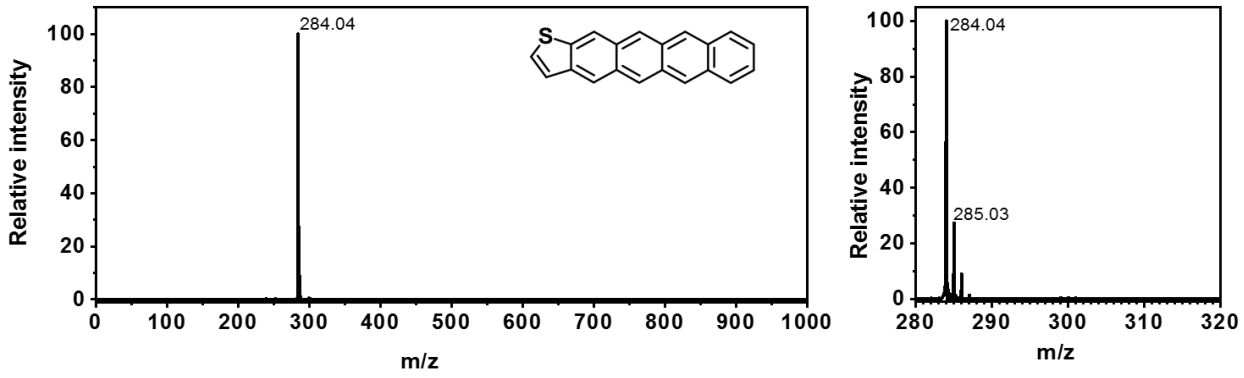

Figure S1-1. Mass spectrometry (MALDITOF-MS Axima Resonance from Shimadzu in LDI-MS mode) of tetraceno[2,3-*b*]thiophene.

Isotopic distribution**:** calc.: 284.06 (100%), 285. 07 (23%), 286.07 (7%)
found: 284.04 (100%), 285. 03 (27%), 286.04 (9%)

Tetraceno[2,3-*b*]thiophene-5,12-dione

Tetraceno[2,3-*b*]thiophene-5,12-dione was obtained from thiophene-3-carbaldehyde and 1,4-dihydroxyanthracene in an aldol condensation reaction using a mixture of ethanol and tetrahydrofuran and 15% NaOH as a base.

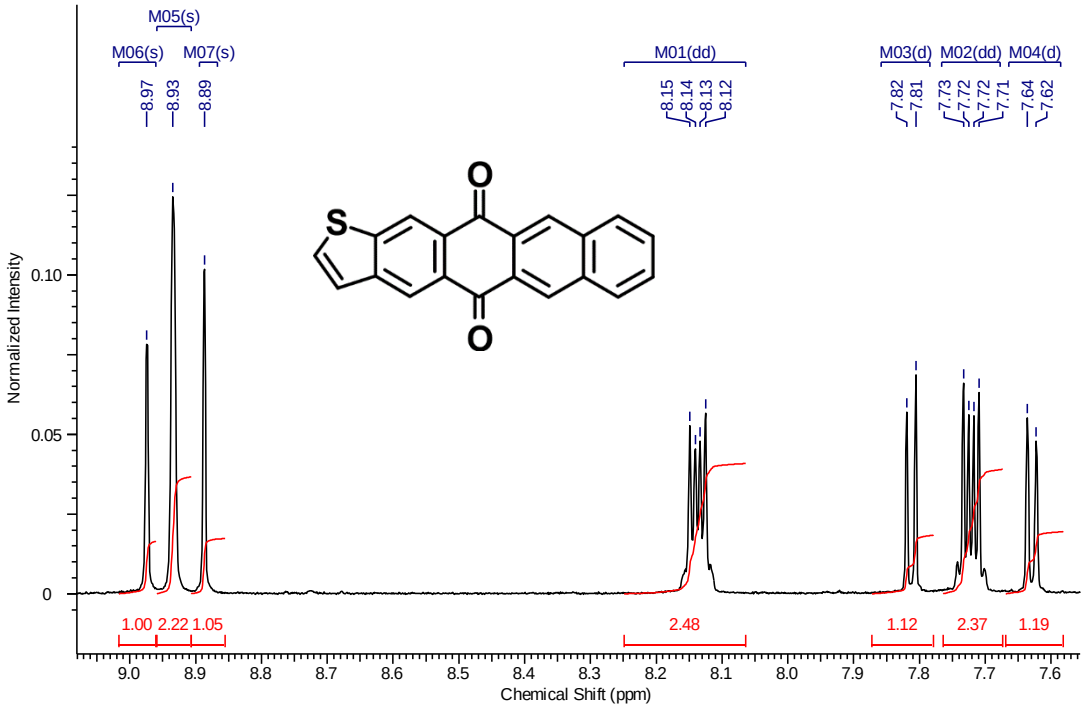

Figure S1-2. ^{1}H-NMR spectrum of tetraceno[2,3-*b*]thiophene-5,12-dione in $CDCl_3$.

Thiophene-2,3-dicarbaldehyde

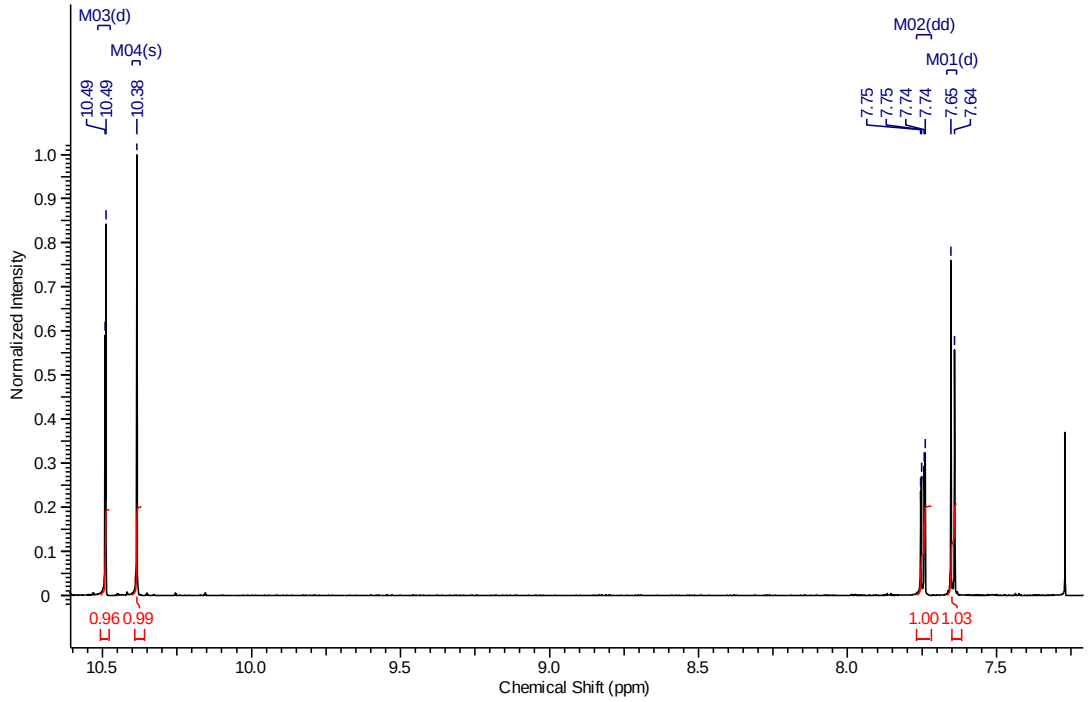

Figure S1-3. ^{1}H-NMR of thiophene-2,3-dicarbaldehyde in $CDCl_3$.

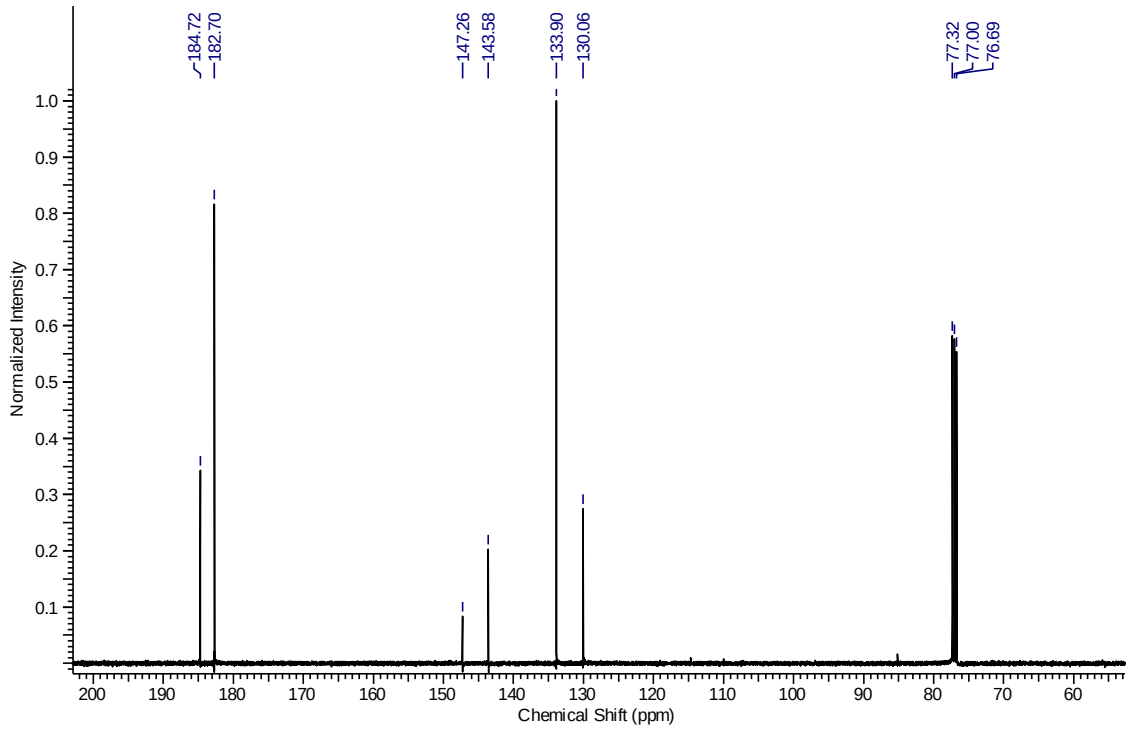

Figure S1-4. ^{13}C-NMR of thiophene-2,3-dicarbaldehyde in $CDCl_3$.

1,4-Anthracenedione

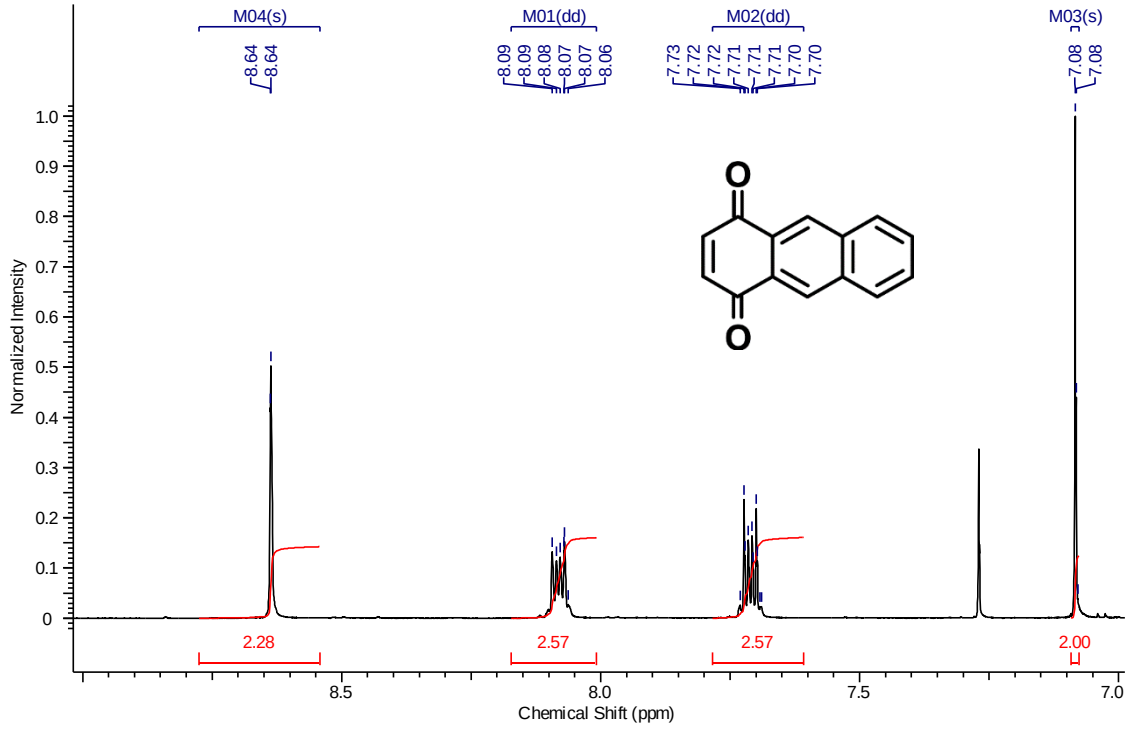

Figure S1-5. ^{1}H-NMR of 1,4-anthracenedione in $CDCl_3$.

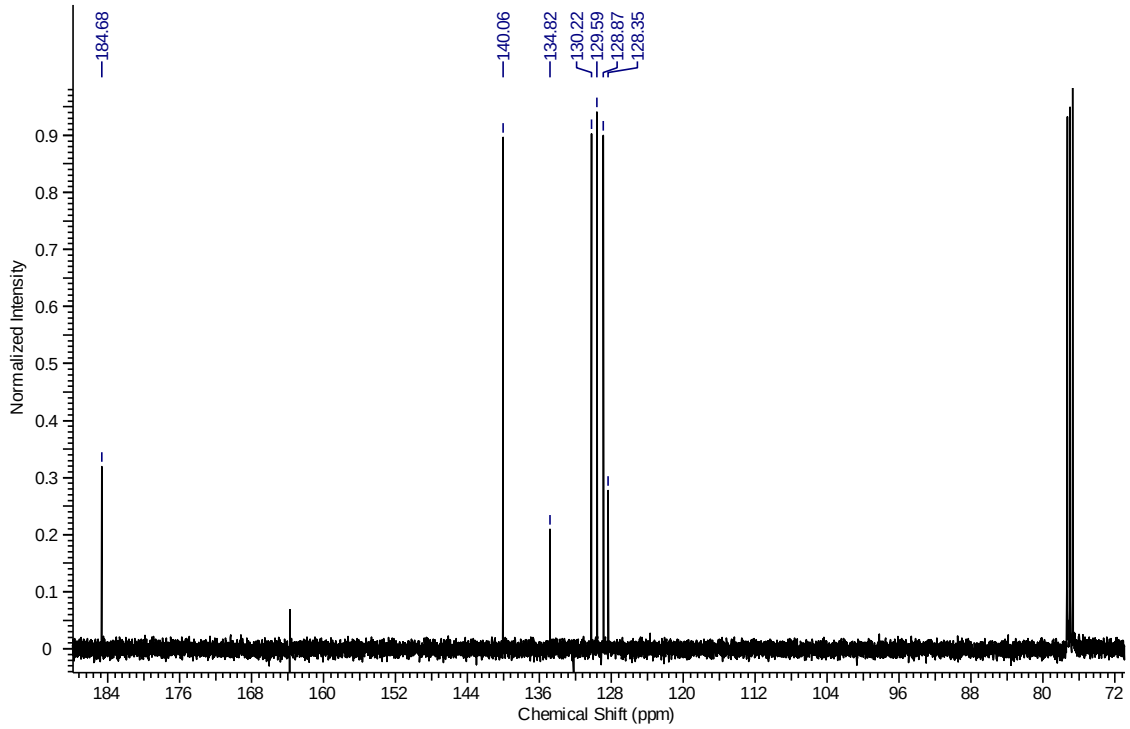

Figure S1-6. ^{13}C-NMR of 1,4-anthracenedione in $CDCl_3$.

[SI1] U. Kraft, J. E. Anthony, E. Ripaud, M. A. Loth, E. Weber, H. Klauk, *Chem. Mater.* **2015**, 27, 998-1004.

2. Thermally induced desulfurization reaction of tetracenothiophene on Cu(111)

When tetracenothiophene (TCT) molecules are adsorbed on Cu(111) above room temperature, they strongly interact with the metallic surface, inducing the desulfurization reaction of the thiophene unit. When deposited with the substrate at a temperature below 280 K, all TCT molecules are found intact on the surface (Figure S2a), while for deposition temperatures above 320 K, all molecules are desulfurized and bound to the substrate through covalent bonds, forming the TC-D derivative. The TC-D molecules appear in the STM images with a lower density-of-states at the reacted side (Figure S2b). This thermally induced reaction is similar to the case of other thiophene-containing molecules desulfurized on metallic substrates [SI2-SI4].

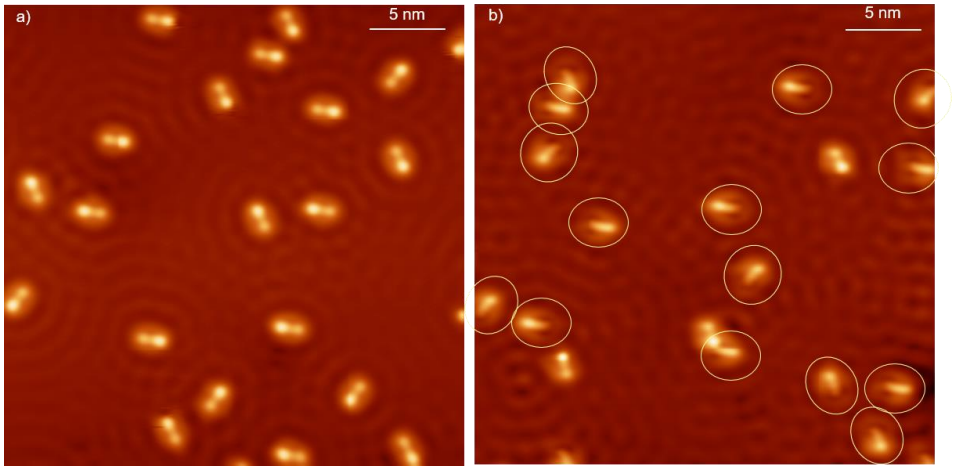

Figure S2. STM images of TCT molecules deposited onto a Cu(111) surface held at temperatures of 270 K (a) and 310 K (b), respectively. The TC-D molecules produced by the desulfurization reaction of TCT are encircled.

[SI2] J. Stöhr, J. L. Gland, E. B. Kollin, R. J. Koestner, A.L. Johnson, E. L. Muetterties, F. Sette, *Phys. Rev. Lett.* **1984**, *53*, 2161-2164.

[SI3] L. E. Dinca, J. M. MacLeod, J. Lipton-Duffin, C. Fu, D. Ma, D. F. Perepichka, F. Rosei, *J. Phys. Chem. C* **2015**, *119*, 22432-22438.

[SI4] L. E. Dinca, C. Fu, J. M. MacLeod, J. Lipton-Duffin, J. L. Brusso, C. E. Szakacs, D. Ma, D. F. Perepichka, F. Rosei, *ACS Nano* **2013**, *7*, 1652-1657.

3. Electric-field induced desulfurization reaction of tetracenothiophene

The thiophene unit of the TCT molecules can be desulfurized producing the TC-D molecules by using the precise control of the tip position in STM and the electric field applied across the STM tunnel junction. In Figure S3 are presented the STM images of a TCT and the resulted TC-D molecules.

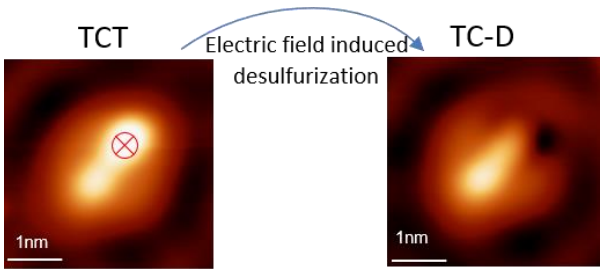

Figure S3. STM images of TCT and the resulted TC-D molecules by a desulfurization reaction induced by the electric field applied between the surface and the STM tip placed above the thiophene unit marked in the left image.

4. Conductance measurements as a function of tip-sample distance

Formation (interruption) of a contact between the tetracene terminal of the TCT molecule and the tip apex occurs spontaneously while approaching (retracting) the tip towards (from) the afore-mentioned tetracene terminal along the *z* axis, in a relative distance range of 0 to 500 pm of the approach distance (Figure S4-1). In Figure S4-1a, after completion of the G(z) measurement, the TCT molecule is picked up from the surface and remains on the apex of the tip. In Figure 4-1b, when the tip is retracted and reaches a certain z distance, the tip-molecule contact is interrupted and the molecule falls back onto the surface and remains there. The conductance through the molecular system (G_M) is extracted from the step height of the $G/G_0(z)$ data in the jump-to-contact regime. The conductance has similar values in the tip-sample distance range considered for the data set.

Figure S4-2a shows the conductance values (averaged for a bin size of ±5 pm) as a function of the tip-sample distance. The average conductance values are larger for TC-D compared to TCT for the entire range of distances where the tip-molecule contact is formed or broken, *i.e.* for any geometry of the molecular junction (*e.g.*, with different ratios between suspended and flat-lying parts of the molecule).

The conductance histograms of the TCT and TC-D species shown in the manuscript depict the conductance values obtained in the window of 50 pm corresponding to relative distances of [-365;-315] pm of the tip approach (Figure S4-2b). In this small distance range (small compared to the lengths of the molecules, which are 14.54 Å (pentacene), 14.29 Å (TCT) and 14.20 Å (TC-D) according to our DFT calculations), the geometry of the entire junction changes negligibly for each measurement, allowing for a better comparison of the conductance values.

Despite the limited number of measurement points, the parameters of the mathematical apparatus used to find the peak positions have little to no influence on the peak positions, thus confirming the reliability of the analysis and the calculated difference in conductance. Figure S4-3 shows the conductance histograms with different binning size, extracted from the jump-to-contact curves in the *z* interval [-365;-315] pm relative to the set point. The binning size does not affect the conductance values of the two types of molecules.

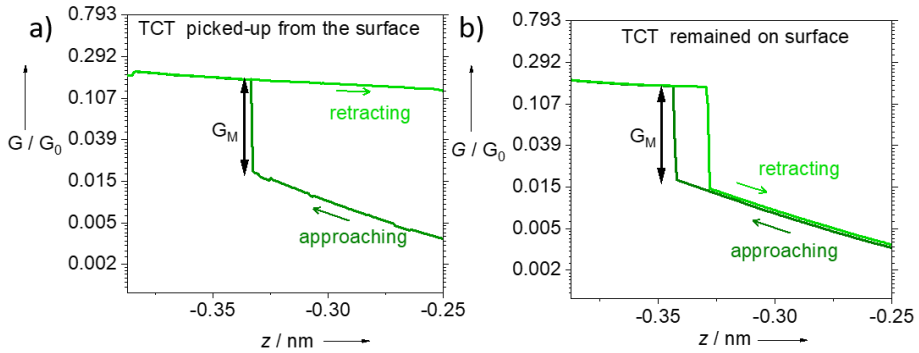

Figure S4-1. G(z) curves acquired by approaching the tip towards the molecule and then retracting it from the surface, for the case when the molecule remains at the tip apex (a) or on the surface (b). The conductance through the molecular system G_M is obtained by subtracting the tunneling conductance measured just before the jump-to-contact from the value measured just after the jump-to-contact.

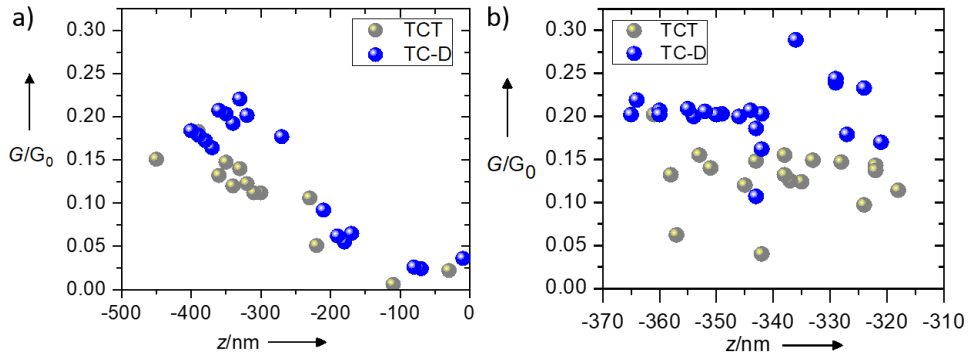

Figure S4-2. a) Average conductance values (with a bin size of ±5 pm) measured for the interval [-500;0] pm of the tip-approach distance where tip-molecule contact was formed or broken.
b) Conductance values (not averaged) measured in the window of 50 pm corresponding to the interval range of [-365;-315] pm.

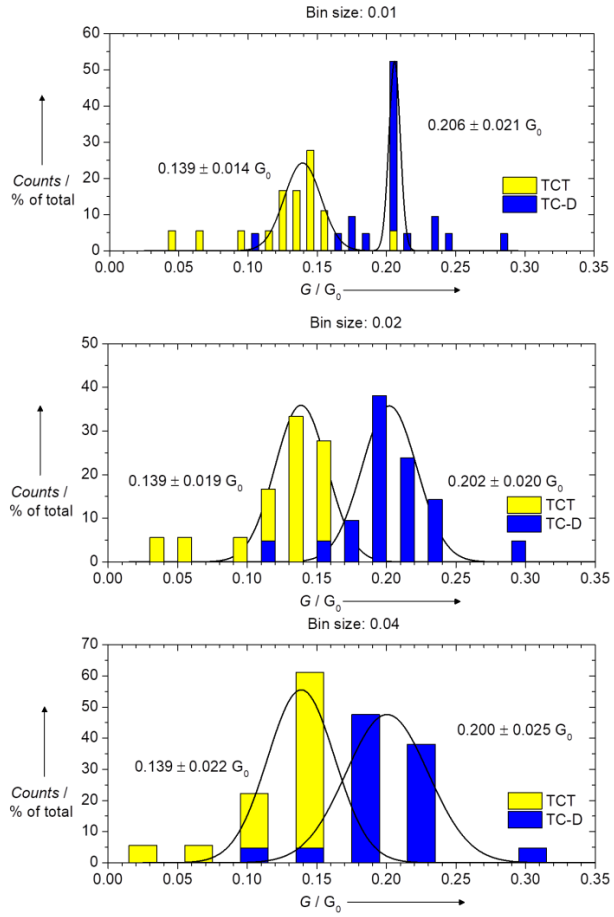

Figure S4-3. Conductance histograms, with different binning size, arranged in vertical panels, obtained in the approaching regime with the Gaussian distribution for the TCT and the TC-D molecules. The error bar corresponds to the standard deviation extracted from the Gaussian fit.

5. Interaction strength at the metal-organic interface

The experimental evidence that the TC-D molecules are anchored to the metal surface more strongly than the TCT molecules is theoretically supported by the C-Cu distances displayed in Figure S5 and by the interaction energies of the molecules with the Cu surface. The optimized geometries clearly show shorter C-Cu distances for the TC-D molecular structure, highlighting a shorter adsorption distance on the surface and a stronger binding. The interaction energies of the molecular structures with the Cu(111) surface, E^{int}, were computed as:

$$E^{int} = E^{total} - (E^{surf} + E^{mol}),$$

where E^{total} is the total energy of the molecule/surface system, E^{surf} the total energy of the clean surface, and E^{mol} the total energy of the molecule in the gas phase (in its adsorbed geometry). A substantial increase in interaction energy with the surface from -3.53 eV for the TCT molecule and -3.79 eV for the pentacene molecule to -13.55 eV for the TC-D molecule is found, thus supporting the experimental findings.

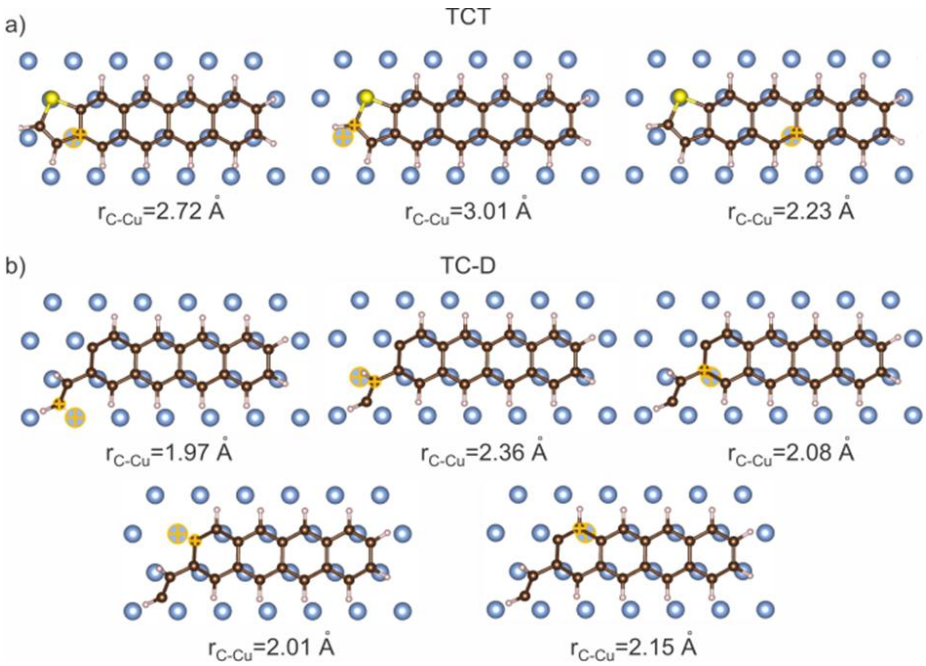

Figure S5. Typical C-Cu distances for the TCT molecule (a) and the TC-D molecule (b), respectively. The two atoms involved in the measured bond are displayed with yellow crosses in the ball-and-stick representations.

Author Contributions

U.S., H.K. and K.K. conceived this project. B.B., P.W., U.S. and K.K. designed the experiments. T.M., B.B., V.S., I.P. and M.P. carried out the sample preparation and performed the experiments. T.M., B.B. analyzed the experimental data. U.K. and H.K. carried out the molecule synthesis. P.M and P.J. performed the potential map simulations. R.P. and A.A performed the DFT calculations. All authors contributed to and discussed the manuscript.